DETECTING NON-OBVIOUS SECONDARY CRATERS ON THE MOON.

L.R. Ostrach[1], K.N. Singer[2], N.E. Petro[1], M.S. Robinson[3], [1]NASA Goddard Space Flight Center, Greenbelt, MD; [2]Southwest Research Institute, Boulder, CO; [3]School of Earth and Space Exploration, Arizona State University, Tempe, AZ.(lillian.r.ostrach@nasa.gov)

Introduction: Identifying secondary craters within a region used to measure crater size-frequency distributions (SFDs) is critical for appropriate age determination (relative and absolute). Recent investigations [1,2] indicate that secondaries do not always display typical features (e.g., chains, overlapping clusters), suggesting that "non-obvious" secondaries dominate SFDs at diameters ≤1 km [3], particularly in the lunar mare. Here, we build upon a previous analysis of the density of impact craters in Mare Imbrium [4] to investigate clusters of circular, non-overlapping impact craters that are candidate far-flung, non-obvious secondaries.

Methods: Crater SFDs for all circular, non-overlapping impact craters with diameters $D \geq 500$ m were measured on LROC WAC 100 m/pixel mosaics for a region encompassing 2.27×10^5 km^2 within Mare Imbrium. Crater density was determined from a point density calculation according to the methodology of Ostrach and Robinson [4]. Varying the neighborhood radius during the density calculation alters the spatial structure observed in the density map; small neighborhood radii emphasize local, statistical variations. Therefore, systematic local trends in groupings of craters, which are expected for clusters of non-obvious far-flung secondaries, will be apparent. Locations with candidate non-obvious secondaries identified in the crater density map were then investigated through morphology, and potential source craters were predicted by expected secondary crater size distribution relative to the parent crater. Estimates of the maximum secondary size at a given range from a primary were derived from the power-law quantile regression fitting of measured secondary crater fields [5].

Results: The density map [**Fig. 1**] indicates locations for candidate non-obvious secondaries, identified by linear-like regions of high density. Measurements of the crater diameters within the clusters identified in the density map interpreted to be secondaries range from 500 m to ~2 km. Some clusters of craters are within a higher albedo region than the surrounding terrain (ejecta ray) and are traced back to a probable parent primary [i.e., Copernicus], consistent with origin as a secondary impact. For other clusters of craters, size-range distributions estimate the maximum secondary size at a given distance from a primary [**Fig. 2**; 5]; several parent craters likely contribute to the expansive rays and secondary crater chains observed, including Copernicus, Aristillus, Autolycus, Aristarchus, and in one case, Aristoteles [**Fig. 3**].

Discussion: What is the effect of including these far-flung secondaries in crater SFDs? Obvious second-ary craters, those that display typical features, are typically recognized and excluded from measurements, along with the surface area they cover. However, clusters of circular, non-overlapping craters are not as easily identified as "typical" secondaries. The inclusion of these craters has the potential not only to contaminate the SFDs but also to over-predict the small primary crater production function. Secondary contamination was considered for the lunar chronology, with an estimated <10% uncertainty for the standard distribution curve between 0.8–3 km [6,7]. However, a recent reassessment [8] indicates that earlier investigations suffered from images with non-uniform illumination conditions as well as the effects of lower resolution on crater identification. Typically, absolute ages for the mare are determined from craters with $D \geq 1$ km to limit inclusion of potential secondaries [e.g., 3,6-9]. Although the presence of non-obvious secondaries with $D \geq 1$ km is estimated to constitute <5% of craters of comparable size [e.g., 10], high-resolution image data enable new, quantitative assessments of lunar secondary populations and enable improved measurements (and thus age determination) for the primary craters at these smaller diameters.

Conclusions and Future Work: Candidate clusters of non-obvious secondary craters (500 m to ~2 km in diameter) were identified in Mare Imbrium through measures of crater density. Observations of morphology and size-range distribution estimates indicate that several parent craters likely contribute to these clusters of craters in Mare Imbrium. Additional observations of morphology in LROC NAC images are required to determine whether the clustered craters have similar degradation states (similar ages), because it is possible that the clusters are comprised of craters of different ages (superposed younger primaries or secondaries). Nonetheless, measures of crater density aid in the identification and determination of clustered non-obvious secondaries, and it is probable that at least some portion of the clustered non-overlapping craters in Mare Imbrium represent far-flung, non-obvious secondaries, similar to those observed at Tycho [2] and Zunil [on Mars; 1].

Candidate clusters of non-obvious secondaries can be identified in crater density maps and their probable parent primary determined from secondary crater size distributions. These techniques provide improvements in identification of secondary craters, particularly previously unrecognized clustered non-obvious secondaries, and enable an improved quantitative assessment of the secondary population, and therefore more accurate ages, on the Moon.

References: [1] McEwen, A.S. et al. (2005) Icarus 176, 351–381. [2] Dundas, C.M. and McEwen, A.S. (2007) Icarus 186, 31–40. [3] McEwen, A.S. and Bierhaus, E.B. (2006) Ann. Rev. Earth Planet. Sci. 34, 535–567. [4] Ostrach, L.R. and Robinson, M.S. (2014) Lunar Planet. Sci. Conf. 45, abstract 1266. [5] Singer, K.N. et al. (2014) Lunar Planet. Sci. Conf. 45, abstract 1162. [6] Neukum, G. et al. (1975) The Moon 12, 201–229. [7] Neukum, G. et al. (2001) Space Sci. Rev. 96, 55–86. [8] Robbins, S.J. (2014) EPSL, 403, 188–198. [9] Hartmann, W.K. et al. (1981) In: BVTP, 1049–1127. [10] Werner, S.C. et al. (2009) Icarus, 200, 406–417.
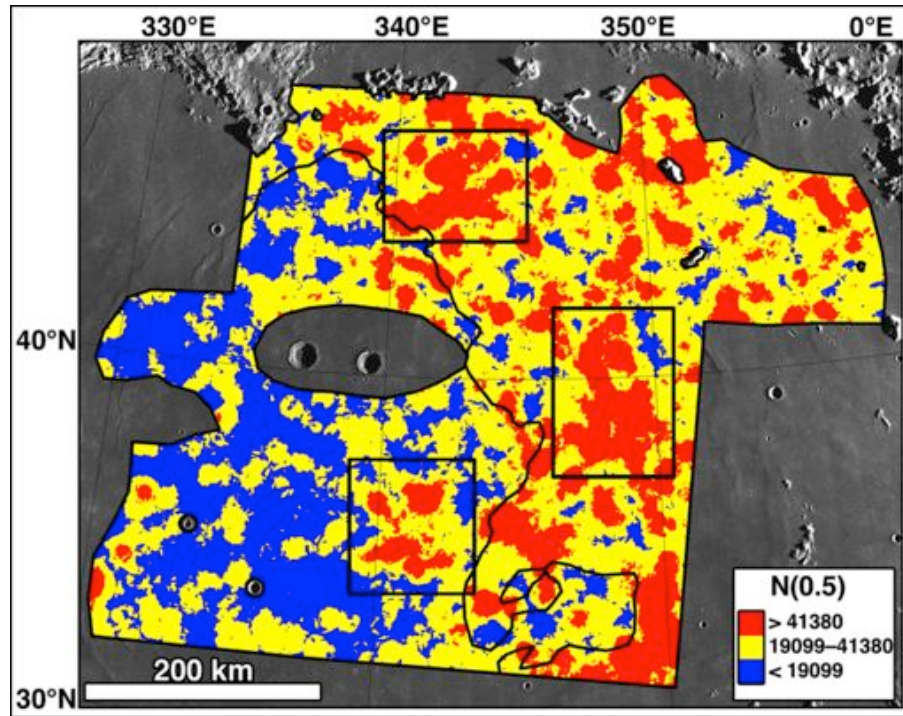
Fig. 1. Density of impact craters for craters with $D \geq 500$ m (2.27×10^5 km^2 measurement area); output cell size is 1 km and neighborhood radius is 10 km. This region is centered on and encompasses a distinct multispectral boundary between Imbrian-aged and Eratosthenian-aged basalts; this boundary is observed in measures of crater density derived from larger neighborhood sizes [5]. Here, a small neighborhood size emphasizes local clustering trends that may reflect non-obvious secondaries contaminating the crater measurements. Boxes surround three locations of candidate non-obvious secondaries. Density map overlaid on LROC WAC mosaic centered at 45.0°N, 340.0°E in Mare Imbrium.
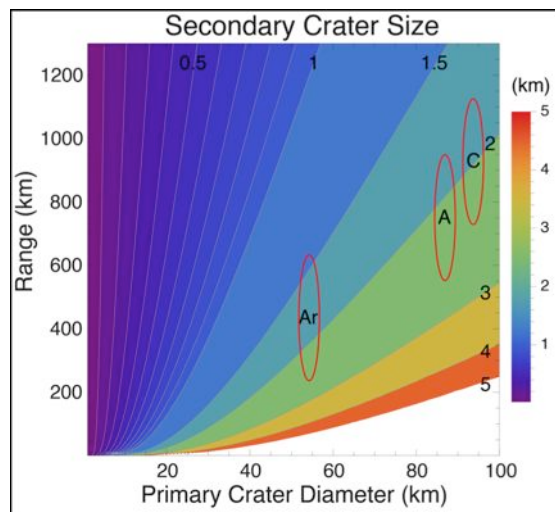

Fig. 2. Predicted secondary crater diameter (km; color) as a function of both primary crater diameter and distance (Range) from the parent primary. Red ellipses centered on primary D (Aristillus, Aristoteles, and Copernicus) and distance from crater center to the center of the study region (33.0°N, 345.0°E), extending ±200 km from the region center point. Differences between this estimate and the size-range distributions [**Fig. 3**] reflect differences between individual craters and the generalized regression fits [5].
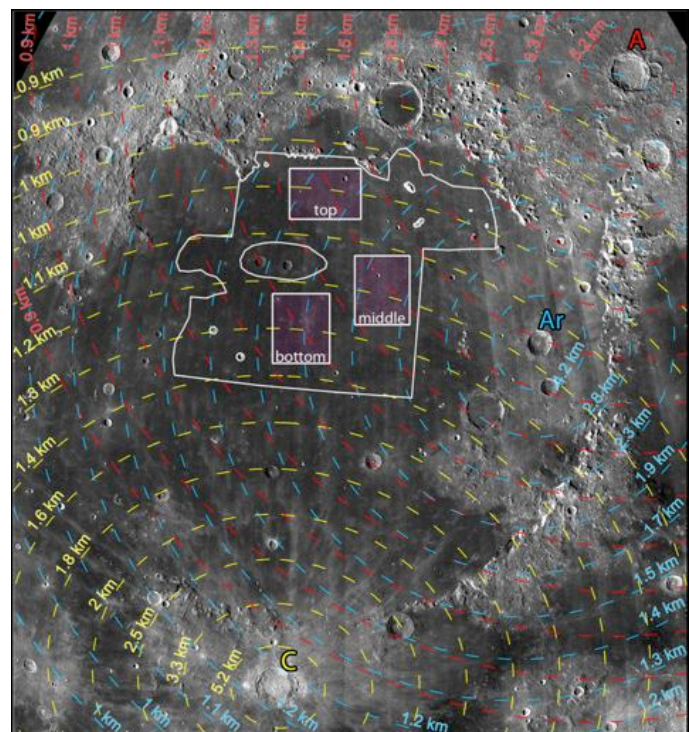

Fig. 3. Secondary size-range distributions predict the maximum secondary crater size at 100 km radial interval ranges from Aristillus (Ar; cyan), Aristoteles (A; red), and Copernicus (C; yellow). Shaded boxes are the three regions in the figures above. Derived from quantile regression fits to secondary crater field measurements [5].